Soluble Synthetic Multiporphyrin Arrays. 3. Static Spectroscopic and Electrochemical Probes of Electronic Communication

Jyoti Seth,[†] Vaithianathan Palaniappan,[†] Richard W. Wagner,[‡] Thomas E. Johnson,[‡] Jonathan S. Lindsey,[‡] and David F. Bocian*[,†]

Contribution from the Department of Chemistry, University of California, Riverside, California 92521, and Department of Chemistry, North Carolina State University, Raleigh, North Carolina 27695

Received May 14, 1996[⊗]

Abstract: A comprehensive electrochemical (cyclic and square-wave voltammetry, coulometry) and static spectroscopic (absorption, resonance Raman (RR), electron paramagnetic resonance (EPR)) study is reported for a series of dimeric and trimeric porphyrin-based arrays. All the arrays consist of tetraarylporphyrins linked via ethyne groups at the *p*-positions of the aryl rings. The complexes investigated include zinc-free base and bis-zinc dimers which contain varying degrees of torsional constraint between the porphyrin rings and the aryl group of the linker, and linear and right-angle trimers in which two zinc porphyrins are bridged by either a zinc or free base porphyrin. The spectroscopic studies were performed on singly and multiply oxidized complexes as well as the neutral species. The electrochemical and spectral properties of the arrays indicate that the electronic communication between the macrocycles is relatively weak in the ground and excited electronic states. This communication is through-bond, rather than through-space, and is mediated by the diarylethyne linker. In the case of the torsionally unconstrained dimers, unusually large RR intensity enhancements are observed for aryl-ring and ethyne-bridge stretching modes. The RR intensity enhancements are attributed to an excited-state conformational change that enhances the conjugation between the π-electron systems of the porphyrin ring and bridging diarylethyne group. The intensity of the aryl and ethyne-bridge vibrations monotonically decreases as the degree of torsional constraint increases. This trend parallels the decrease in energy-transfer rates observed for these arrays (unhindered, $\sim(24\ \text{ps})^{-1}$; monohindered, $\sim(46\ \text{ps})^{-1}$; bis-hindered $\sim(88\ \text{ps})^{-1}$) and indicates that the excited-state electronic communication can be tuned via structural modification of the diarylethyne linker. In contrast, the optical and RR signatures of the linear and right-angle trimeric arrays are essentially identical indicating that the geometrical arrangement of the porphyrins does not significantly influence the excited-state communication. The half-wave potentials for oxidation of the zinc porphyrins in the dimers and trimers are essentially identical. The EPR spectra of the oxidized arrays exhibit complex temperature-dependent signatures that reflect hole/electron hopping and/or spin exchange interactions in the ground electronic state. Hole/electron hopping in all the monocations is rapid ($10^7\ \text{s}^{-1}$ or faster) on the EPR time scale in liquid solution and slow in frozen solution. Neither the degree of torsional constraint (dimers) nor the geometrical arrangement of the constituent porphyrins (trimers) has any affect on the EPR signatures of the monocations indicating that this structural element does not affect ground-state electronic communication as reflected in hole/electron hopping rates. Exchange interactions in the multiply oxidized arrays are significant (probably 1000 MHz or greater) in both liquid and frozen solutions and, in certain cases, are enhanced upon solvent freezing. Unlike the hole/electron hopping, the exchange interactions in the dimers are influenced by the degree of torsional constraint. In contrast, the geometrical arrangement of the constituent porphyrins in the trimers has no measurable effect on this property. Collectively, the static spectroscopic and electrochemical studies provide new insights into the electronic communication pathways in the diarylethyne-linked multiporphyrinic arrays.

I. Introduction

Photosynthetic organisms use light-harvesting complexes to capture sunlight and funnel the energy to the reaction center.[1] The energy transfer process is highly efficient even though it occurs over long distances and involves hundreds of chromophores.[2] The elucidation of the structural and electronic properties of natural light-gathering arrays is an important objective of photosynthesis research but may also provide a foundation for the design of synthetic molecular devices for use in photovoltaic energy conversion/charge storage,[3] photosensitization,[4] and optical sensing,[5] funneling,[6a] transmission,[6b] and gating.[6c]

[†] University of California.

[‡] North Carolina State University.

[⊗] Abstract published in *Advance ACS Abstracts,* November 1, 1996.

(1) (a) Larkum, A. W. D.; Barrett, J. *Adv. Bot. Res.* **1983**, *10*, 1−219. (b) *Photosynthetic Light-Harvesting Systems*; Scheer, H., Schneider, S., Eds.; W. deGruyter: Berlin, 1988. (c) Mauzerall, D. C.; Greenbaum, N. L. *Biochim. Biophys. Acta* **1989**, *974*, 119−140. (d) Hunter, C. N.; van Grondelle, R.; Olsen, J. D. *Trends Biochem. Sci.* **1989**, *14*, 72−76.

(2) (a) Sundstrom, V.; van Grondelle, R. In *The Chlorophylls*; Scheer, H., Ed.; CRC Press: Boca Raton, FL, 1991; pp 1097−1124. (b) Holzwarth, A. R. *Ibid*, pp 1125−1152.

(3) (a) Gregg, B. A.; Fox, M. A.; Bard, A. J. *J. Phys. Chem.* **1990**, *94*, 1586−1598. (b) Liu, C.-Y.; Pan, H.-L.; Fox, M. A.; Bard, A. J. *Science* **1993**, *261*, 897−899.

(4) (a) Pandey, R. K.; Vincente, G. H.; Shiau, F. Y.; Dougherty, T. J.; Smith, K. M.; *Proc. SPIE Int. Soc. Opt. Eng.* **1991**, *1426*, 356−361. (b) Pandey, R. K.; Shiau, F. Y.; Meunier, I.; Ramaprasad, S.; Sumlin, A. B.; Dougherty, T. J.; Smith, K. M. *Proc. SPIE Int. Soc. Opt. Eng.* **1992**, *1645*, 264−273. (c) Pandey, R. K.; Shiau, F. Y.; Ramachandran, R.; Dougherty, T. J.; Smith, K. M. *J. Chem. Soc., Perkin Trans. 1* **1992**, 1377−1385.

(5) (a) Anderson, H. L.; Martin, S. J.; Bradley, D. D. C. *Angew. Chem. Int. Ed. Engl.* **1994**, *33*, 655−657. (b) Anderson, H. L. *Inorg. Chem.* **1994**, *33*, 972−981.

S0002-7863(96)01613-7 CCC: $12.00

The detailed determination of the factors governing the functional characteristics of naturally occurring light-harvesting systems is difficult owing to the size and complexity of the assemblies. Consequently, synthetic porphyrin-based model systems are essential for probing the effects of molecular organization on electronic communication.[5−17] Recently, one of our groups developed a synthetic strategy for preparing large arrays of covalently linked porphyrins which exhibit the physical and architectural properties required of a viable light-harvesting system.[6,17] In a previous report, we examined the mechanism(s) of electronic communication in several of these synthetic arrays including dimers and pentamers (including an energy funnel[6a]) and their monomeric building blocks. These studies utilized electrochemical (cyclic and square-wave voltammetry, coulometry) and static spectroscopic (absorption, resonance Raman (RR), electron paramagnetic resonance (EPR)) techniques.[18] The spectroscopic studies were performed on singly and multiply oxidized complexes as well as the neutral species. These studies revealed that the electronic communication between the diarylethyne-linked porphyrins is weak in both the ground and excited electronic states, as expected due to the large distances between the porphyrin units (center-to-center distances ∼20 Å; edge-to-edge distances ∼13 Å). Nevertheless, electronic communication appears to be primarily through-bond rather than through-space. This property facilitates rapid energy transfer between adjacent components in the array (<100 ps)[19] but does not lead to deleterious electron transfer quenching reactions. Efficient energy transfer without competing electron transfer is one of the hallmarks of effective light harvesting systems.

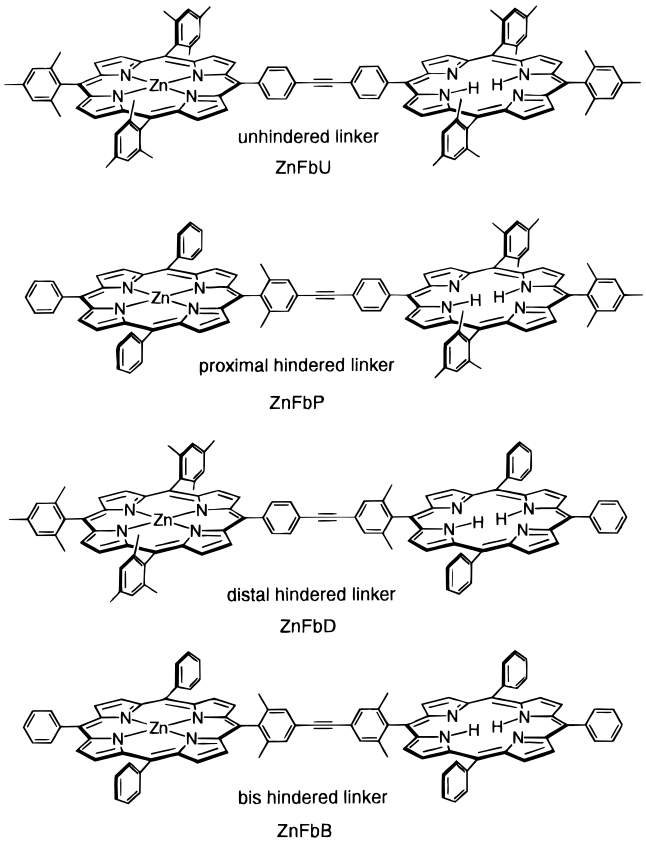

Figure 1. Structures of the zinc−free base dimeric arrays.

In this paper, we extend our electrochemical and static spectroscopic studies of the arrays to a series of zinc−free base (ZnFbU, ZnFbP, ZnFbD, ZnFbB) and bis-zinc (Zn_2U, Zn_2M, Zn_2B) dimers containing varying degrees of torsional constraint between the porphyrin rings and the aryl groups in the linker. The structures of these dimers are shown in Figures 1 and 2, respectively. The zinc−free base dimers are the same as those for which detailed energy-transfer measurements are reported in Paper 2 of this series.[19] These dimers exhibit energy-transfer rates which depend on the degree of torsional constraint ranging from ∼$(24\ ps)^{-1}$ in ZnFbU to ∼$(88\ ps)^{-1}$ in ZnFbB. The studies on the torsionally constrained dimers afford the opportunity for correlating the static spectroscopic and energy-transfer properties. We also examined the redox and spectroscopic properties of linear (ZnFbZn−L, Zn_3L) and right-angle (ZnFbZn−R, Zn_3R) trimers that contain two zinc porphyrins bridged either by another zinc porphyrin or a free base porphyrin. The structures of these arrays are shown in Figure 3. The two types of trimeric arrays represent architectural motifs which are both present in star-shaped pentameric arrays.[18] The studies of the trimers provide a test of the influence of linear versus right-angle arrangements of the constituent porphyrins on electronic communication. Taken together, the electrochemical and spectroscopic studies provide additional insights

(6) (a) Prathapan, S.; Johnson, T. E.; Lindsey, J. S. *J. Am. Chem. Soc.* **1993**, *115*, 7519−7520. (b) Wagner, R. W.; Lindsey, J. S. *J. Am. Chem. Soc.* **1994**, *116*, 9759−9760. (c) Wagner, R. W.; Lindsey, J. S., Seth, J.; Palaniappan, V.; Bocian, D. F. *J. Am. Chem. Soc.* **1996**, *118*, 3996−3997.

(7) (a) Wasielewski, M. R. In *The Chlorophylls*; Scheer, H., Ed.; CRC Press: Boca Raton, FL, 1991; pp 269−286. (b) Wasielewski, M. R. *Chem. Rev.* **1992**, *92*, 435−461.

(8) (a) Gust, D.; Moore, T. A. *Top. Curr. Chem.* **1991**, *159*, 103−151. (b) Gust, D.; Moore. T. A. *Adv. Photochem.* **1991**, *16*, 1−65. (b) Gust, D.; Moore, T. A.; Moore, A. L.; Gao, F.; Luttrull, D.; DeGraziano, J. M.; Ma, X. C.; Makings, L. R.; Lee, S.-J.; Trier, T. T.; Bittersmann, E.; Seely, G. R.; Woodward, S.; Bensasson, R. V.; Rougee, M.; DeSchryver, F. C.; Van der Auwaraer, J. *J. Am. Chem. Soc.* **1991**, *113*, 3638−3649.

(9) (a) Won, Y.; Friesner, R. A.; Johnson, M. R.; Sessler, J. L. *Photosynth. Res.* **1989**, *45*, 4767−4784. (b) Sessler, J. L.; Johnson, M. R.; Creager, S. E.; Fettinger, J. C.; Ibers, J. A. *J. Am. Chem. Soc.* **1990**, *112*, 9310−9329. (c) Sessler, J. L.; Capuano, V. L.; Harriman, A. *J. Am. Chem. Soc.* **1993**, *115*, 4618−4628.

(10) (a) Helms, A.; Heiler, D.; McLendon, G. *J. Am. Chem. Soc.* **1992**, *114*, 6227−6238. (b) Helms, A.; Heiler, D.; McLendon, G. *J. Am. Chem. Soc.* **1991**, *113*, 4325−4327. (c) McLendon, G. *Acc. Chem. Res.* **1988**, *21*, 160−167.

(11) (a) Osuka, A.; Maruyama, K. *J. Am. Chem. Soc.* **1988**, *110*, 4454−4456. (b) Osuka, A.; Maruyama, K. *J. Am. Chem. Soc.* **1990**, *112*, 3054−3059. (c) Osuka, A.; Maruyama, K.; Mataga, N.; Asahi, T.; Yamazaki, I.; Tamai, J. *J. Am. Chem. Soc.* **1990**, *112*, 4958−4959. (d) Nagata, T.; Osuka, A.; Maruyama, K. *J. Am. Chem. Soc.* **1990**, *112*, 3054−3059. (e) Osuka, A.; Nagata, T.; Maruyama, K. *Chem. Lett.* **1991**, 481−484. (f) Osuka, A.; Nagata, T.; Maruyama, K. *Chem. Lett.* **1991**, 1687−1690. (g) Osuka, A.; Liu, B.-L.; Maruyama, K. *Chem. Lett.* **1993**, 949−952.

(12) (a) Brun, A. M.; Harriman, A.; Heitz, V.; Sauvage, J.-P. *J. Am. Chem. Soc.* **1991**, *113*, 8657−8663. (b) Brun, A. M.; Atherton, S. J.; Harriman, A.; Heitz, V.; Sauvage, J.-P. *J. Am. Chem. Soc.* **1992**, *114*, 4632−4639.

(13) (a) Wasielewski, M. R.; Niemczyk, M. P.; Svec, W. A. *Tetrahedron Lett.* **1982**, *23*, 3215−3218. (b) Abdalmuhdi, I.; Chang, C. K. *J. Org. Chem.* **1985**, *50*, 411−413. (c) Seta, P.; Bienvenue, E.; Maillard, P.; Momenteau, M. *Photochem. Photobiol.* **1989**, *49*, 537−543.

(14) (a) Milgrom, L. R. *J. Chem. Soc., Perkin Trans. 1* **1983**, 2335−2339. (b) Davila, J.; Harriman, A.; Milgrom, L. R. *Chem. Phys. Lett.* **1987**, *136*, 427−430. (c) Wennerstrom, O.; Ericsson, H.; Raston, I.; Svensson, S.; Pimlott, W. *Tetrahedron Lett.* ***1989***, *30*, 1129−1132.

(15) (a) Anderson, S.; Anderson, H. L.; Sanders, J. K. M. *Acc. Chem. Res.* **1993**, *26*, 469−475. (b) Anderson, H. L.; Sanders, J. K. M. *J. Chem. Soc., Chem. Commun.* **1989**, 1714−1715. (c) Anderson, S.; Anderson, H. L.; Sanders, J. K. M. *Angew. Chem., Int. Ed. Engl.* **1992**, *31*, 907−910.

(16) (a) Lin, V. S.-Y.; DiMagno, S. G.; Therien, M. J. *Science* **1994**, *264*, 1105−1111. (b) Angiolillo, P. J.; Lin, V. S.-Y.; Vanderkooi, J. M.; Therien, M. J. *J. Am. Chem. Soc.* **1995**, *117*, 12514−12527.

(17) (a) Lindsey, J. S.; Prathapan, S.; Johnson, T. E.; Wagner, R. W. *Tetrahedron* **1994**, *50*, 8941−8968. (b) Wagner, R. W.; Johnson, T. E.; Li, F.; Lindsey, J. S. *J. Org. Chem.* **1995**, *60*, 5266−5273. (c) Paper 1 of this series: Wagner, R. W.; Johnson, T. E.; Lindsey, J. S. *J. Am. Chem. Soc.* **1996**, *118*, 11166−11180.

(18) Seth, J.; Palaniappan, V.; Johnson, T. E.; Prathapan, S.; Lindsey, J. S.; Bocian, D. F. *J. Am. Chem. Soc.* **1994**, *116*, 10578−10592.

(19) Paper 2 of this series: Hsiao, J.-S.; Krueger, B.; Wagner, R. W.; Johnson, T. E.; Delaney, J. K.; Mauzerall, D. C.; Fleming, G. R.; Lindsey, J. S.; Bocian, D. F.; Donohoe, R. J. *J. Am. Chem. Soc.* **1996**, 118, 11181−11193.

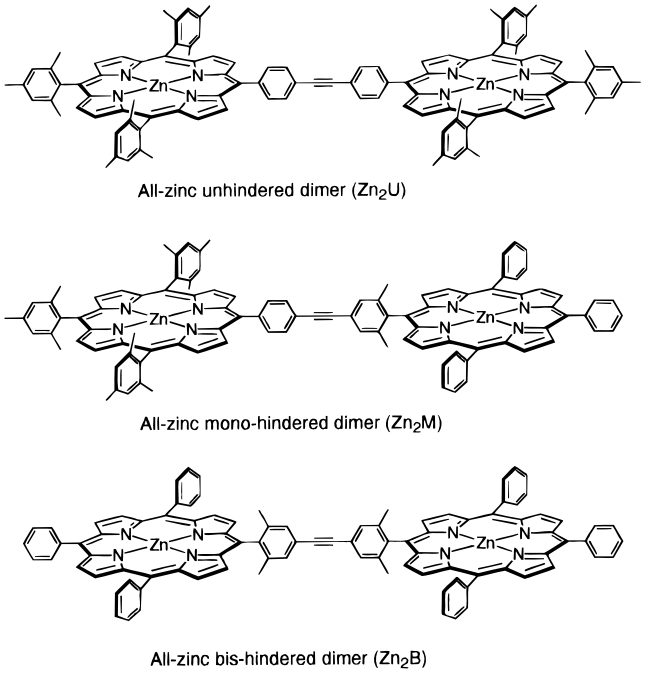

Figure 2. Structures of the bis−zinc dimeric arrays.

into the electronic and photophysical properties of the diarylethyne-linked arrays.

II. Experimental Section

The various porphyrin arrays were synthesized and characterized by methods previously described.[17] The electrochemical and spectroscopic studies were performed on samples prepared in CH_2Cl_2 (dimers) or in a 3:1 v/v mixture of $CHCl_3$:CH_2Cl_2 (trimers). The trimers exhibit reasonable solubility in $CHCl_3$ but relatively low solubility in CH_2Cl_2. The solvent mixture was used because neat $CHCl_3$ is a poor solvent for electrochemical studies. CH_2Cl_2 and $CHCl_3$ (both Aldrich, HPLC Grade) were purified by vacuum distillation from P_2O_5 followed by another distillation from CaH_2. For the electrochemical studies, tetrabutylammonium hexafluorophosphate (TBAH; Aldrich, recrystallized three times from methanol and dried under vacuum at 110 °C) was used as the supporting electrolyte. The solvents were degassed thoroughly by several freeze−pump−thaw cycles prior to use.

The oxidized complexes were prepared in a glovebox (Vacuum Atmospheres HE-93 equipped with a Model 493 Dri-Train) by using standard electrochemical instrumentation (PAR 175 Universal Programmer and PAR 173 potentiostat or EG&G 263 potentiostat/galvanostat). The samples were contained in a three compartment cell equipped with a Pt wire working electrode, a Pt mesh counter electrode, and a Ag/Ag^+ (butyronitrile) reference electrode. The oxidized species were generated by quantitative coulometric bulk electrolysis at a Pt mesh electrode. The integrity of the samples was checked by cyclic voltammetry after each successive oxidation. In all cases, the cyclic voltammograms were reproducible upon repeated scans and exhibited no scan rate dependence in the 20−100 mV/s range. Upon oxidation, the samples were transferred within the glovebox to an optical cuvette (absorption) or quartz capillary (RR and EPR) and carefully sealed in the glovebox. All of the spectroscopic studies on the oxidized complexes were performed immediately following the oxidation. Prior to obtaining RR and EPR spectra, absorption spectra were recorded to reconfirm the integrity of the samples.

The absorption spectra of the neutral and oxidized complexes were recorded with a diode array spectrometer (Hewlett-Packard 8254A). All spectra were obtained at ambient temperature. The sample concentration was typically 0.01 mM.

The RR spectra of the neutral and oxidized species were recorded with a triple spectrograph (Spex 1877) equipped with either a 1200 or 2400 groove/mm holographically etched grating in the third stage. A liquid-nitrogen-cooled, UV-enhanced 1152 × 298 pixel charge coupled device (Princeton Instruments, LN/CCD equipped with an EEV1152-UV chip) was used as the detector. The RR experiments were conducted at both ambient and low (15 K) temperatures. For the latter experiments, the sample was mounted on the cold tip of a closed cycle He refrigeration system (ADP Cryogenics, DE-202 Displex). The sample concentration for all the RR experiments was typically 0.05 mM. The excitation wavelengths were provided by the output of an Ar ion (Coherent Innova 400−15UV) laser. The Raman shifts were calibrated by using the known values of indene, fenchone, and CH_3-CN. The Raman shifts are accurate to ± 1 cm^{-1} for strong and/or isolated bands. The laser power at the sample was typically 5−7 mW for the ambient temperature experiments and less than 1 mW for the low-temperature experiments. The spectral resolution was ~ 2 cm^{-1} at a Raman shift of 1600 cm^{-1}.

The EPR spectra were recorded with an X-band spectrometer (Bruker ER200D) equipped with a NMR gaussmeter (Bruker ER035M) and a microwave frequency counter (Hewlett-Packard 3550B). The EPR spectra were obtained at ambient and low temperature. The low-temperature studies (100−295 K) were performed with a continuous flow N_2 cryostat (Bruker). The sample concentration for all the experiments was typically 0.05 mM. The microwave power and magnetic field modulation amplitude were typically 5.7 mW and 0.32 G, respectively.

III. Results

A. Neutral Complexes. (1) Absorption Spectra. The ambient-temperature absorption spectra of neutral ZnFbU and ZnFbB are shown as the solid traces in the left top and bottom panels, respectively, of Figure 4. The analogous spectra of Zn_2U and Zn_2B are shown in the right panels. The spectral features of the arrays with bis-hindered linkers are very similar to those containing the unhindered linker. This is also the case for the arrays containing the mono-hindered linkers (not shown). The absorption spectra of ZnFbP, ZnFbD, and ZnFbB are approximately a superposition of the absorption spectra of the zinc and free base porphyrins as was previously reported for ZnFbU.[18] Collectively, these results indicate that the addition of the torsional constraints on the aryl ring(s) of the linker does not significantly alter the structure of the porphyrin ring or result in discernible changes in the electronic coupling between the constituent porphyrins of the array. The latter result is not surprising given that ZnFbU and Zn_2U, for which the electronic coupling should be the largest among the series of arrays, exhibit absorption characteristics which are similar to those of monomeric porphyrins, indicative of the relatively weak electronic coupling in all the diarylethyne-linked arrays.[18]

The ambient-temperature absorption spectra of neutral ZnFbZn−L and ZnFbZn−R are shown as the solid traces in the left top and bottom panels, respectively, of Figure 5. The analogous spectra of Zn_3L and Zn_3R are shown in the right panels. The spectra of the trimeric arrays are qualitatively similar to one another and similar to those of the dimeric arrays. However, the B-band maxima of all the trimers are slightly red shifted (4−6 nm) relative to those of the monomers. In both linear trimers, the B-bands exhibit asymmetries (ZnFbZn−L) or splittings (Zn_3L) which are not as pronounced in the right-angle trimers. These effects are absent in the Q-band region where the spectra of the trimers are essentially identical with those of the dimers. The red-shifts and splittings of the B-bands in the trimeric arrays (4−6 nm) are comparable to those we have previously observed in star-shaped diarylethyne-linked pentameric arrays. The perturbations of the B-band are indicative of excitonic interactions between the porphyrins in the arrays.[9a,11d,e,20−23]

(20) Kasha, M.; Rawls, H. R.; El-Bayoumi, M. A. *Pure Appl. Chem.* **1965**, *11*, 371−392.
(21) Gouterman, M.; Holten, D.; Lieberman, E. *Chem. Phys.* **1977**, *25*, 139−153.

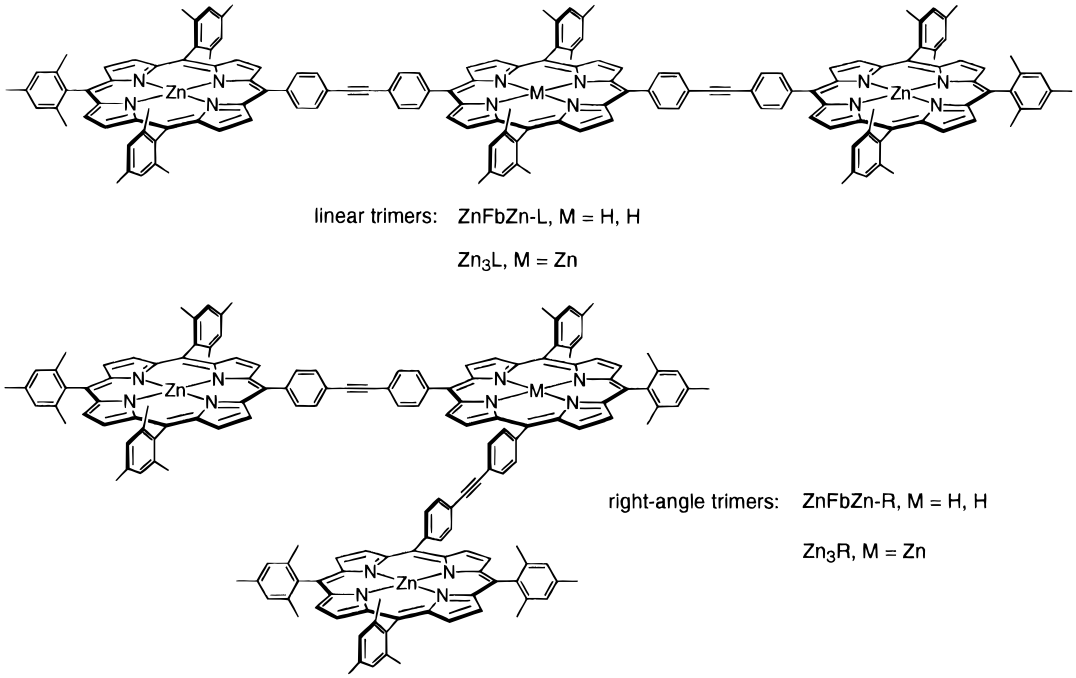

Figure 3. Structures of the trimeric arrays.

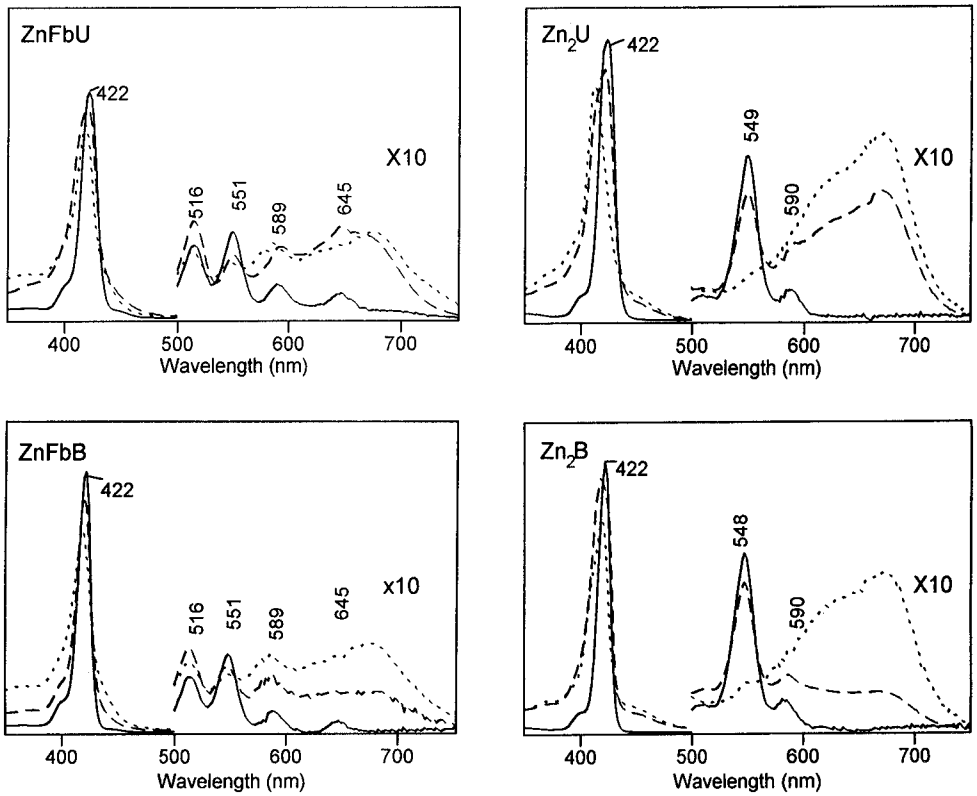

Figure 4. Absorption spectra of the neutrals (solid lines), monocations (dashed lines), and dications (dotted lines) of the zinc−free base (left panel) and bis-zinc (right panel) dimeric arrays obtained at 295 K. The spectra shown are for the arrays containing the unhindered (top) and bis-hindered (bottom) linkers. The spectra of the arrays containing the monohindered linker (not shown) are similar. The spectra in the 500−750-nm range are scaled by a factor of 10 to facilitate comparison.

(2) RR Spectra. The high-frequency regions of the ambient-temperature B-state-excitation (λ_{ex} = 457.9 nm) RR spectra of neutral ZnFbU, ZnFbP, ZnFbD, and ZnFbB are shown in the left panel of Figure 6. The analogous RR spectra of Zn_2U, Zn_2M, and Zn_2B are shown in the left panel of Figure 7. The scattering characteristics of the porphyrin skeletal modes of the different arrays are generally unremarkable. In contrast, the effects of torsional constraint on the aryl ring mode, ν_{aryl},[24] at

(22) Hunter, C. A.; Sanders, J. K. M.; Stone, A. J. *Chem. Phys.* **1989**, *133*, 395−404.

(23) Schick, G. A.; Schreiman, I. C.; Wagner, R. W.; Lindsey, J. S.; Bocian, D. F. *J. Am. Chem. Soc.* **1989**, *111*, 1344−1350.

(24) (a) Burke, J. M.; Kincaid, J. R.; Spiro, T. G. *J. Am. Chem. Soc.* **1978**, *100*, 6077−6083. (b) Burke, J. M.; Kincaid, J. R.; Peters, S.; Gagne, R. R.; Collman, J. P.; Spiro, T. G. *J. Am. Chem. Soc.* **1978**, *100*, 6083−6088 (c) Li, X.-Y.; Czernuszewicz, R. S.; Kincaid, J. R.; Su, Y. O.; Spiro, T. G. *J. Phys. Chem.* **1990**, *94*, 31−47. (d) Schick, G. A.; Bocian, D. F. *J. Am. Chem. Soc.* **1983**, *105*, 1830−1838.

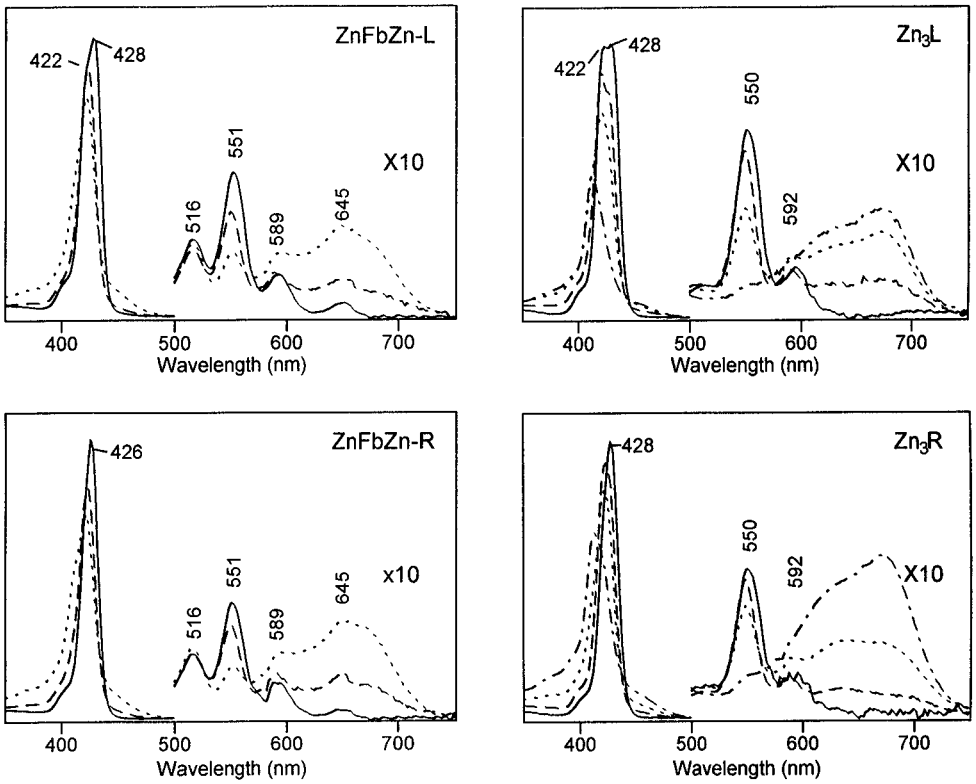

Figure 5. Absorption spectra of the neutrals (solid lines), monocations (dashed lines), dications (dotted lines), and trications (dashed-dotted lines) of the trimeric dimeric arrays obtained at 295 K. The spectra in the 500−750-nm range are scaled by a factor of 10 to facilitate comparison.

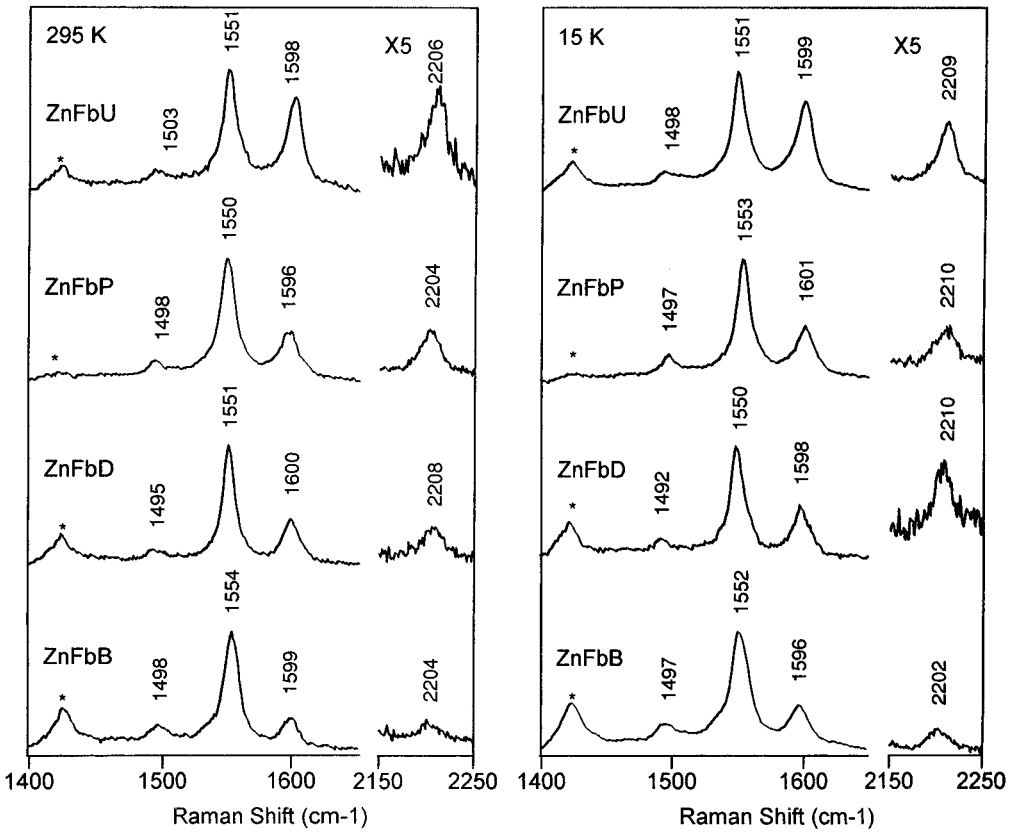

Figure 6. B-state-excitation (λ_{ex} = 457.9 nm) RR spectra of the neutral zinc−free base dimeric arrays obtained at 295 K (left panel) and 15 K (right panel). The bands marked by asterisks are due to solvent.

~1600 cm^{-1} and the ethyne stretching mode, $\nu_{C\equiv C}$,[18] at ~2210 cm^{-1} are noteworthy. As was discussed in our earlier studies of diarylethyne-linked porphyrin arrays, the RR intensity of the ν_{aryl} mode of porphyrins containing an unhindered diarylethyne group is unusually large, as much as 10 times greater (depending on the array) than in tetraarylporphyrins which do not contain this group.[18] The fact that the $\nu_{C\equiv C}$ vibration of unhindered diarylethyne-substituted complexes exhibits significant RR intensity enhancement is even more remarkable considering that this group is five bonds away from the porphyrin π-system.

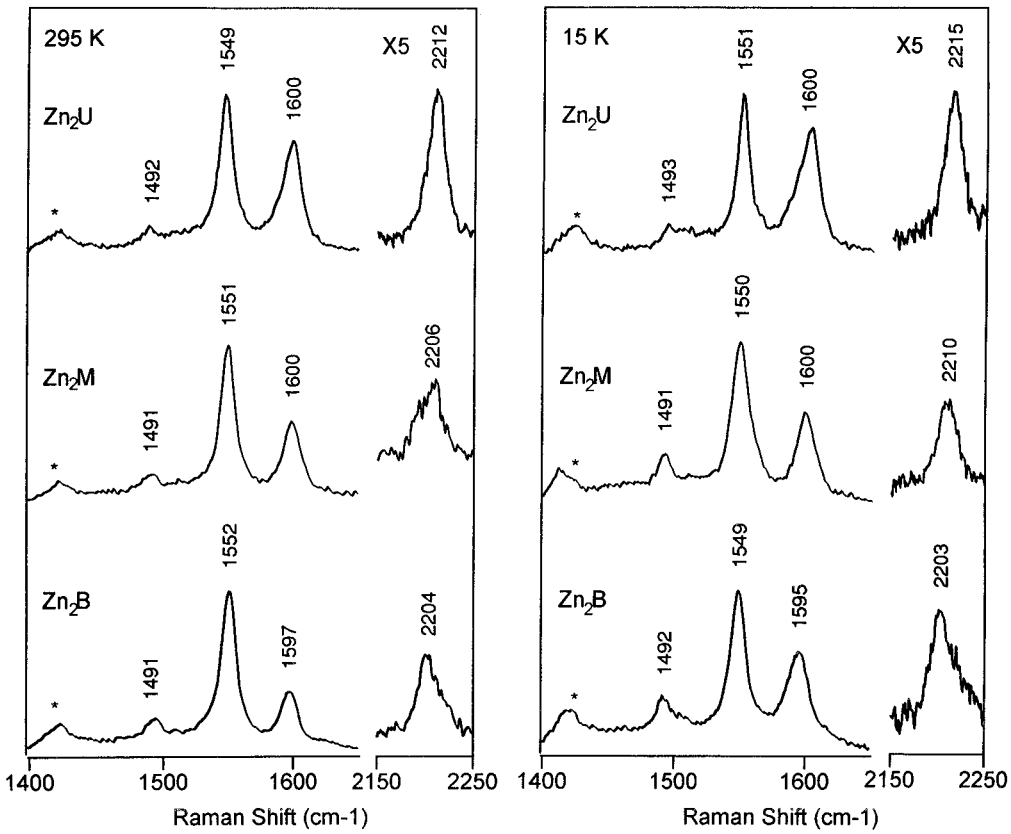

Figure 7. B-state-excitation (λ_{ex} = 457.9 nm) RR spectra of the neutral bis-zinc dimeric arrays obtained at 295 (left panel) and 15 K (right panel). The bands marked by asterisks are due to solvent.

The large RR enhancement of the ν_{aryl} and $\nu_{C\equiv C}$ vibrations of ZnFbU and Zn_2U is evidenced by their significant intensity compared with the ν_2 porphyrin ring-skeletal mode at ~1550 cm^{-1} (Figures 6 and 7, top traces). The ν_{aryl} and $\nu_{C\equiv C}$ modes of Zn_2U appear to be somewhat stronger than those of ZnFbU. As torsional constraints are added to the diarylethyne linker, the RR intensity of the ν_{aryl} and $\nu_{C\equiv C}$ modes of both the zinc−free base and bis-zinc arrays monotonically decreases. The intensity decreases are most dramatic in the case of the zinc−free base dimeric arrays (Figure 6). For ZnFbP and ZnFbD, the intensity of both ν_{aryl} and $\nu_{C\equiv C}$ is approximately 50% of that for ZnFbU (using ν_2 as a reference). For ZnFbB, the intensities of both RR bands are approximately 25% of that for ZnFbU. As a consequence, the intensity of ν_{aryl} for ZnFbB is similar to that of tetraarylporphyrins which do not contain the diarylethyne group and $\nu_{C\equiv C}$ is barely visible above the noise. In the case of the bis-zinc dimeric arrays (Figure 7), the structurally induced RR intensity decreases of ν_{aryl} and $\nu_{C\equiv C}$ are less pronounced. For Zn_2M, the modes exhibit ~60−70% of their intensity in Zn_2U. [The intensity of $\nu_{C\equiv C}$ is somewhat difficult to quantitate because of the noise characteristics on the band.] For Zn_2B, the intensities are ~50−60% of those of Zn_2U. These results suggest that the factors which determine the RR intensity behavior of the ν_{aryl} and $\nu_{C\equiv C}$ modes differ somewhat in the zinc−free base versus bis-zinc dimeric arrays.

In order to investigate whether the RR enhancements of the ν_{aryl} and $\nu_{C\equiv C}$ vibrations are affected by temperature, the RR spectra of the dimeric arrays were also examined at cryogenic termperatures. Representative low-temperature (15 K) RR spectra of the zinc−free base and bis-zinc dimeric arrays are shown in the right panels of Figures 6 and 7, respectively. Comparison of the ambient- and low-temperature RR data reveals that for both the zinc−free base and bis-zinc dimeric arrays containing the unhindered and monohindered linkers, the effects of temperature appear to be relatively minor. For these arrays, there may be some changes in the relative intensities of ν_{aryl} and $\nu_{C\equiv C}$ versus ν_2; however, these intensity changes are difficult to quantitate, particularly for the $\nu_{C\equiv C}$ mode. On the other hand, for both ZnFbB and Zn_2B, the intensities of ν_{aryl} and $\nu_{C\equiv C}$ exhibit a temperature sensitivity which is outside the range of experimental error. In particular, these modes are more intense at low temperature. This is especially apparent in the case of Zn_2B for which both modes increase in intensity by ~50%. The intensity gain is less dramatic for ZnFbB and is ~20%. Together, these observations indicate that *ortho*-substitution of both aryl groups in the linker gives rise to a temperature dependence of the structural properties of the linker which is absent (or less significant) in the less torsionally constrained dimers.

The high-frequency regions of the ambient-temperature B-state-excitation (λ_{ex} = 457.9 nm) RR spectra of the neutral linear and right-angle trimeric arrays are shown in Figure 8. The spectra of the various trimers are generally similar to one another and similar to those of the corresponding zinc−free base and bis-zinc dimeric arrays. The trimeric arrays, all of which contain an unhindered diarylethyne linker, exhibit strongly enhanced ν_{aryl} and $\nu_{C\equiv C}$ modes. The intensity of these modes appears to be slightly larger in the Zn_3L and Zn_3R compared with ZnFbZn−L and ZnFbZn−R. This trend parallels that observed for the bis-zinc versus zinc−free base dimers (vide supra). The similarity between the RR spectra of the linear and right-angle trimers indicates that these different arrangements of the constituent porphyrins have negligible influence on the structural and electronic properties of the arrays.

B. Oxidized Complexes. The rationale for investigating the oxidized arrays was to gain insight into the effects of torsional constraint (dimers) and linear versus right-angle porphyrin arrangements (trimers) on the rates of hole/electron hopping.[18] These rates are of interest because no independent assessment of the rates of electron transfer is available for the neutral arrays.

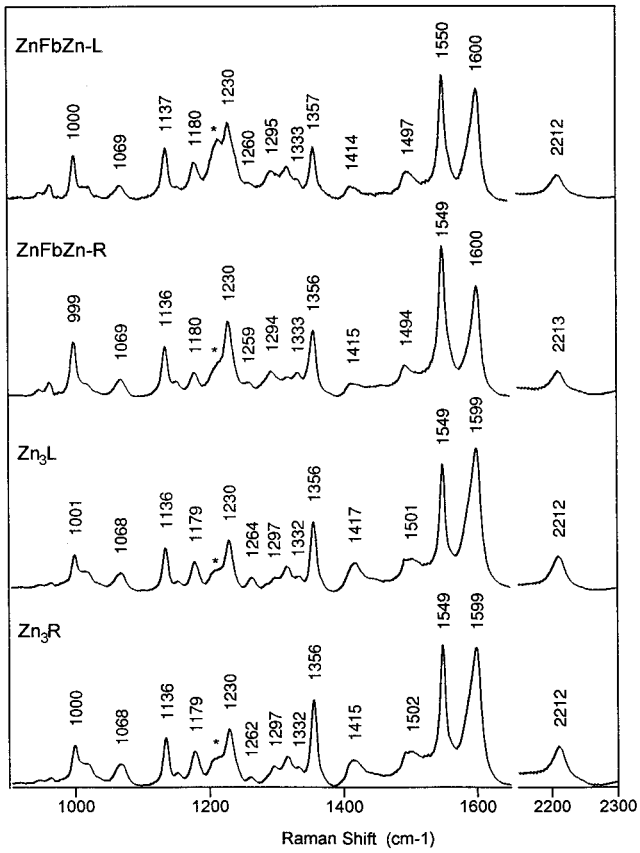

Figure 8. B-state-excitation ($\lambda_{ex} = 457.9$ nm) RR spectra of the neutral trimeric arrays obtained at 295 K. The bands marked by asterisks are due to solvent.

Table 1. Half-Wave Potentials[a] for Oxidation of the Porphyrins of the Various Arrays

	zinc porphyrin		free base porphyrin	
	$E_{1/2}(1)$	$E_{1/2}(2)$	$E_{1/2}(1)$	$E_{1/2}(2)$
ZnFbU[b]	0.63	0.86	0.73	*d*
ZnFbB[b]	0.63	0.86	0.74	1.10
Zn_2U	0.63	0.90		
Zn_2M	0.64	0.89		
Zn_2B	0.64	0.89		
ZnFbZn−L[b]	0.64[c]	0.88[c]	*d*	*d*
ZnFbZn−R[b]	0.67[c]	0.89[c]	0.76	1.11
Zn_3L	0.65[c]	0.90[c]		
Zn_3R	0.65[c]	0.89[c]		

[a] Obtained in CH_2Cl_2 (dimers) or a 3:1 v/v mixture of $CHCl_3$:CH_2Cl_2 (timers) containing 0.1 M TBAH. $E_{1/2}$ *vs* Ag/Ag^+; $E_{1/2}$ of $FeCp_2/FeCp_2^+ = 0.22$ V; scan rate = 0.1 V/s. Values are ±0.01 V. [b] Values are approximate due to overlap of zinc and free base waves. [c] The redox waves due to different zinc porphyrins are not resolved by the cyclic voltammetry. Consequently, only two waves corresponding to the 1st and 2nd ring oxidations are observed. [d] These waves are obscured by the broad zinc $E_{1/2}$ waves.

Although the hole/electron hopping rates in the ground electronic states of the cations are not expected to be equal to the electron-transfer rates in the excited states of the neutrals, they at least provide some measure of the factors which control this type of process.

(1) Electrochemistry. The $E_{1/2}$ values for oxidation of the various dimeric and trimeric arrays are summarized in Table 1. The two $E_{1/2}$ values listed in the table correspond to the first and second oxidations of the porphyrin ring.[25] The redox potentials for the zinc and free base constituents of all the arrays are similar to those of monomeric zinc porphyrins (such as tetraphenylporphyrin and tetramesitylporphyrin) which do not contain a diarylethyne substituent.[18] This behavior reflects the minimal ground-state interaction between the porphyrins in the array and between the porphyrin and ethyne group π-systems. [The $E_{1/2}$ value for oxidation of diphenylethyne is 1.64 V vs SCE[26] and its absorption λ_{max} occurs at ~300 nm,[27] indicating that the highest occupied and lowest unoccupied molecular orbitals of diphenylethyne span those of the porphyrins.]

In the case of the torsionally constrained dimeric arrays, the redox behavior is generally similar to that we have previously reported for ZnFbU and Zn_2U.[18] For the zinc−free base arrays, four overlapping redox waves are observed, two each for the zinc and free base porphyrins. [Electrochemical measurements were not made on ZnFbP and ZnFbD; however, their properties are expected to be similar to those of ZnFbU and ZnFbB.] For the bis-zinc arrays, two redox waves are observed whose peak-to-peak separations are ~70 mV. Quantitative coulometry confirms that each wave corresponds to the removal of two electrons. As is the case for Zn_2U, differential pulse and square-wave voltammetry on Zn_2M and Zn_2B failed to resolve peaks due to the individual one-electron oxidations. However, the peaks exhibit asymmetries which indicate small inequivalences between the redox potentials of the individual zinc porphyrins (50 mV or less). These results are generally consistent with the absorption characteristics of the complexes which are indicative of weak interactions between the porphyrin units.

The redox behavior of the trimeric arrays generally parallels that observed for the dimeric complexes. For ZnFbZn−R, waves are observed at ~0.67, ~0.76, ~0.89, and ~1.11 V. The similarity of the $E_{1/2}$ values to those observed for the zinc−free base dimers suggests that the first and third waves correspond to oxidations of the zinc porphyrin while the second and fourth correspond to oxidation of the free base. Quantitative coulometry of ZnFbZn−R indicates that the lowest potential peak is due to the two overlapped one-electron oxidations of the zinc porphyrins. Square-wave voltammetry shows that this peak is asymmetric. Part of this asymmetry is due to small differences in the $E_{1/2}$ values of the overlapping one-electron oxidations of the two zinc porphyrins and part is due to the proximity of these peaks to the peak from the first oxidation of the free base porphyrin. For ZnFbZn−L only two waves are clearly observed at ~0.64 and ~0.88 V which correspond to the first and second oxidations of the zinc porphyrin. Quantitative coulometry confirms that the lowest potential peak is due to two one-electron oxidations. It is not obvious why the redox waves of the free base porphyrin of ZnFbZn−L are more poorly resolved than those for ZnFbZn−R. Nevertheless the redox potentials for the free base porphyrin of the former array are probably very similar to those of the latter (~0.76 and ~1.11 V). This is supported by the fact that the region between the waves assigned to the zinc porphyrins of ZnFbZn−L is filled in and the higher potential peak exhibits a pronounced asymmetry on the high potential side. In the case of both Zn_3L and Zn_3R, two redox waves are observed at ~0.65 and ~0.90 V. These $E_{1/2}$ values are similar to those observed for the bis-zinc dimeric arrays and are attributed to the first and second oxidations of the zinc porphyrins. Quantitative coulometry on Zn_3L and Zn_3R confirms that the lowest potential waves in fact correspond to three one-electron oxidations. Differential pulse and square-wave voltammetry failed to resolve the peaks due to the structurally distinct (central) porphyrin in either Zn_3R or

(25) (a) Felton, R. H. In *The Porphyrins*; Dolphin, D., Ed.; Academic Press: New York, 1978; Vol. V, pp 53−126. (b) Davis, D. G. *Ibid*., pp 127−152.

(26) Cariou, M.; Simonet, J. *J. Chem. Soc., Chem. Commun.* **1990**, 445−446.

(27) Armitage, J. B.; Entwistle, N.; Jones, E. R. H.; Whiting, M. C. *J. Chem. Soc.* **1954**, 147−154.

Zn_3L. This behavior can be contrasted with that observed for all-zinc pentameric arrays wherein the redox peak due to the central zinc porphyrin could be distinguished from that of the four peripheral zinc porphyrins.[18]

(2) Absorption Spectra. The UV−Vis absorption spectra of the mono- and dications of the dimeric and trimeric arrays are shown along with those of the corresponding neutral complexes in Figures 4 and 5. The spectral characteristics of all of the oxidized complexes are similar to one another and typical of other porphyrin π-cation radicals, namely having weaker, blue-shifted B-bands and very weak, broad bands in the visible and near-infrared regions.[25a] The absorption spectra of the oxidized complexes appear to be a superposition of the spectra of the neutral and cationic species of the different porphyrin units. This observation is consistent with the weak interactions[28−31] between the constituent zinc porphyrins indicated by the electrochemical studies.

The similar $E_{1/2}$ values observed for the one-electron oxidations of the zinc porphyrins in the bis-zinc dimers and all four trimers raises the possibility that the oxidation products could disproportionate into mixtures in which a variety of oxidation states coexist.[32] In the case of bis-zinc dimers, the monocations could disproportionate to yield a neutral and a dication. [The trication of the complexes could also disproportionate.] In the case of the trimer arrays, the disproportionation pattern could be more complicated. It is not possible to determine from the absorption spectra alone whether disproportionation occurs because there are no spectral signatures that distinguish between the various oxidation states of complexes. Regardless, the EPR studies on the arrays show that each of the oxidized species exhibits unique spectral features indicating that no appreciable disproportionation occurs (vide infra). The absence of disproportionation in the torsionally constrained dimers and the various trimers parallels the behavior previously reported for unconstrained bis-dimers and multi-zinc pentameric arrays.[18]

(3) RR Spectra. Exploratory RR studies were conducted on the dications of Zn_2B in order to compare the spectral features with those of Zn_2U. Zn_2B was chosen for the initial studies because the torsional constraints are largest in this array and the neutral parent exhibits the most pronounced temperature dependence in its RR spectra (vide supra). For both $[Zn_2B]^{2+}$ and $[Zn_2U]^{2+}$, B-state-excitation (λ_{ex} = 457.9 nm) RR spectra were examined at ambient (295 K) and low (15 K) temperatures (not shown). The ambient-temperature RR spectral characteristics observed for $[Zn_2B]^{2+}$ were found to be quite similar to those previously reported for $[Zn_2U]^{+}$.[18] In particular, the oxidation products of both arrays exhibit features consistent with formation of $^2A_{2u}$ porphyrin cation radicals (large downshifts in both ν_2 and ν_4)[33] in which the holes are localized on a given porphyrin macrocycle on the RR time scale. In addition, oxidation results in a general decrease in the RR scattering cross section of the porphyrin modes and an increase in the intensities of ν_{aryl} and $\nu_{C\equiv C}$ relative to the porphyrin modes. The frequencies of the ν_{aryl} and $\nu_{C\equiv C}$ vibrations are not, however, affected by oxidation. No additional features were observed in the RR spectra of either $[Zn_2U]^{2+}$ or $[Zn_2B]^{2+}$ upon cooling the samples (not shown). The temperature-dependent trends observed in the spectra of the cations paralleled those observed for the neutral complexes (the RR intensity increases for ν_{aryl} and $\nu_{C\equiv C}$ for Zn_2B at low-temperature but not for Zn_2U). Given that the RR spectral features of $[Zn_2U]^{2+}$ and $[Zn_2B]^{2+}$ did not afford any insights beyond those acquired from studies of the neutral analogs, RR data were not acquired for the oxidation products of the other torsionally constrained dimers or any of the trimers.

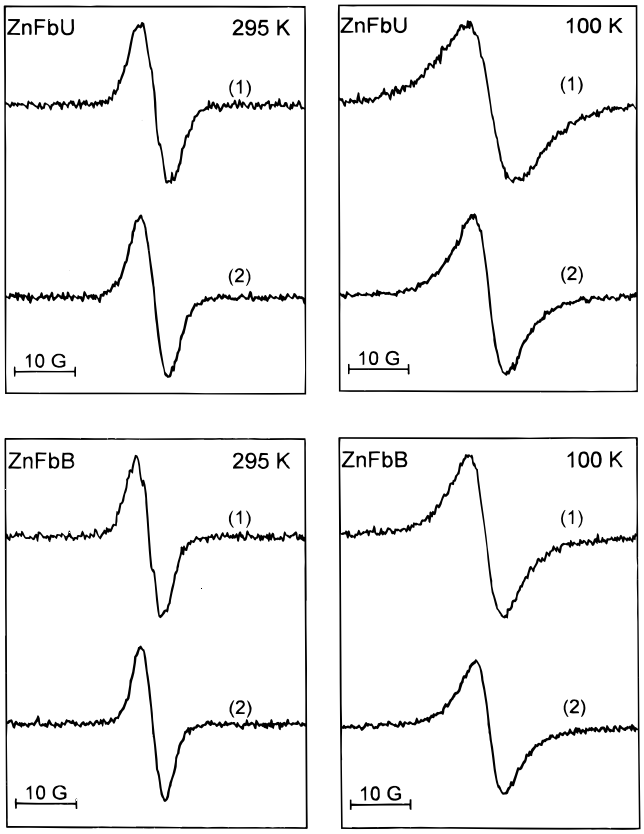

Figure 9. EPR spectra of the mono- (1) and dications (2) of ZnFbU and ZnFbB obtined at 295 and 100 K.

(4) EPR Spectra. The EPR spectra of the mono- and dications of ZnFbU and ZnFbB obtained at 295 and 100 K are shown in Figure 9. The analogous spectra of Zn_2U, Zn_2M, and Zn_2B are shown in Figure 10. The temperature dependences of the nuclear hyperfine splittings or peak-to-peak line widths (when hyperfine structure is not observed) are reported in Table 2. The EPR spectra of all of the cations were examined as a function of sample concentration. No changes in hyperfine splittings or line shape were observed in the concentration range used for the EPR studies ($\leq$0.05 mM). Consequently, the differences observed in the spectral features of the various complexes are intrinsic and cannot be ascribed to intermolecular interactions.

Examination of the EPR signatures for the cations of the various dimeric arrays reveals the following features:

(1) The liquid and frozen solution EPR spectra of $[ZnFbB]^+$ are very similar to those of $[ZnFbU]^+$. Any differences in the magnitude of the $^{14}N_{pyrrole}$ hyperfine splittings ($a^{14}_N \sim 1.6$ G (4.5 MHz))[34] or the line widths for the two arrays at the various temperatures are relatively small. EPR spectra were not

(28) Heath, G. A.; Yellowlees, L. J.; Braterman, P. S. *J. Chem. Soc., Chem. Commun.* **1981**, 287−289.

(29) Elliot, C. M.; Hershenhart, E. *J. Am. Chem. Soc.* **1982**, *104*, 7519−7526.

(30) Edwards, W. D.; Zerner, M. C. *Can. J. Chem.* **1985**, *63*, 1763−1772.

(31) (a) Angel, S. M.; DeArmond, M. K.; Donohoe, R. J.; Wertz, D. W. *J. Phys. Chem.* **1985**, *89*, 282−285. (b) Donohoe, R. J.; Tait, C. D.; DeArmond, M. K.; Wertz, D. W. *Spectrochim. Acta* **1986**, *42A*, 233−240. (c) Tait, C. D.; Macqueen, D. B.; Donohoe, R. J.; DeArmond, M. K.; Hanck, K. W.; Wertz, D. W. *J. Phys. Chem.* **1986**, *90*, 1766−1771. (d) Donohoe, R. R.; Tait, C. D.; DeArmond, M. K.; Wertz, D. W. *J. Phys. Chem.* **1986**, *90*, 3923−3926. (e) Donohoe, R. J.; Tait, C. D.; DeArmond, M. K.; Wertz, D. W. *J. Phys. Chem.* **1986**, *90*, 3927−3930.

(32) Chen, C. H.; Doney, J. J.; Reynolds, G. A.; Saeva, F. D. *J. Org. Chem.* **1983**, *48*, 2757−2761.

(33) Czernuszewicz, R. S.; Macor, K. A.; Li, X.-Y.; Kincaid, J. R.; Spiro, T. G. *J. Am. Chem. Soc.* **1989**, *111*, 3860−3869.

Table 2. Temperature Dependence of the Peak-to-Peak Line Widths/(Hyperfine Splittings)[a] for the 1- and 2-Electron Oxidation Products of Dimeric Arrays

	ZnFbU		ZnFbB		Zn_2U		Zn_2M		Zn_2B	
temp (K)	1	2	1	2	1	2	1	2	1	2
100	7.0	5.9	6.0	4.8	6.0	3.8	6.3	2.2	5.8	1.7
130	7.0	5.9	6.0	4.8	6.0	3.8	6.3	2.2	5.8	1.7
160	7.0	5.9	6.0	4.8	6.0	3.8	6.3	2.2	5.8	1.7
180	(1.6)	4.8	(1.4)	4.9	4.5	4.3	4.7	4.7	4.5	4.5
210	(1.6)	4.8	(1.4)	4.1	4.5	4.1	4.7	4.7	4.5	4.5
240	(1.6)	4.8	(1.4)	4.1	4.2	4.1	4.4	4.4	4.2	4.0
270	5.0[b]	4.5	(1.4)	4.0	3.9	4.0	3.9	4.2	4.2	4.0
295	4.9[b]	4.5	(1.4)	4.0	3.9	4.0	3.9	4.2	3.9	4.0

[a] The line widths/(hyperfine splittings) are ±0.1 G. [b] The line width is approximate due to the unresolved hyperfine.

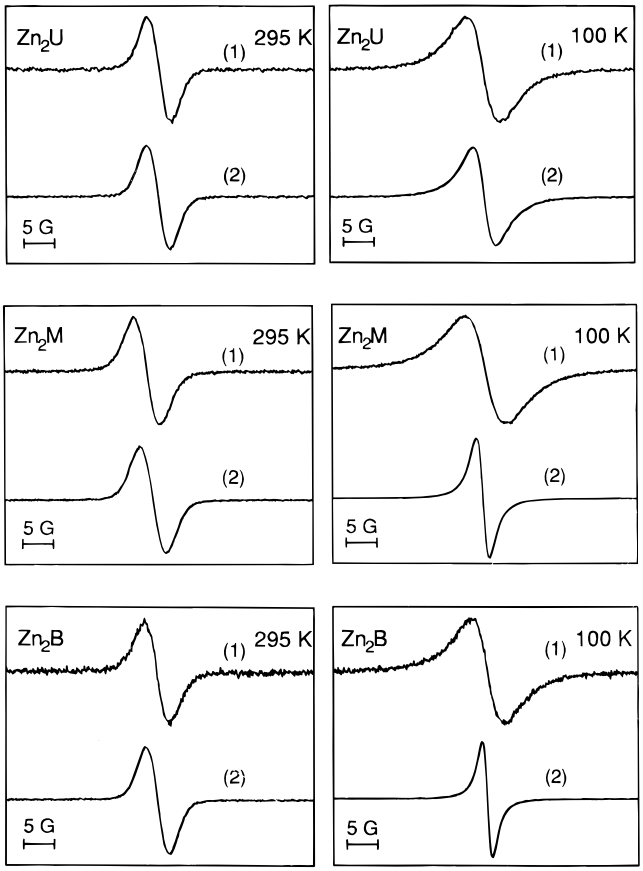

Figure 10. EPR spectra of the mono- (1) and dications (2) of Zn_2U, Zn_2M, and Zn_2B obtained at 295 and 100 K.

recorded for $[ZnFbP]^+$ and $[ZnFbD]^+$ (or their dications); however, the spectral features of these complexes are expected to be similar to those of $[ZnFbU]^+$ and $[ZnFbB]^+$. These observations indicate that the introduction of torsional constraints does not appreciably alter the spin-density distribution in the porphyrin or the location of the hole, which resides exclusively on the zinc porphyrin owing to the relative oxidation potentials of the zinc and free base porphyrins (Table 1). The liquid and frozen solution EPR spectra of $[ZnFbB]^{2+}$ are also qualitatively similar to those of $[ZnFbB]^+$; however the line width is narrower for the former complex. This trend parallels the behavior observed for $[ZnFbU]^{2+}$ versus $[ZnFbU]^+$. There is no evidence for triplet signals in either the $g = 2$ or 4 regions of the EPR spectra of $[ZnFbB]^{2+}$.[35] This observation indicates that the torsional constraints do not significantly alter the dipole−dipole and/or exchange interactions in the biradical.

(2) The liquid and frozen solution EPR signals observed for $[Zn_2M]^+$ and $[Zn_2B]^+$ are essentially identical to those of $[Zn_2U]^+$. No hyperfine structure is resolved for any of these monocations at ambient temperature and the peak-to-peak line width of the unstructured signal is significantly less (∼4.0 G) than that of the full width of the structured signal observed for $[ZnFbU]^+$ and $[ZnFbB]^+$ (∼5.7 G). As the temperature is lowered, the EPR signals for $[Zn_2M]^+$ and $[Zn_2B]^+$ broaden. Below the freezing point of the solvent, the line width of the EPR signals for $[Zn_2M]^+$ and $[Zn_2B]^+$ is independent of temperature and similar to that observed for $[ZnFbU]^+$ and $[ZnFbB]^+$ (∼6.0−7.0 G). The full widths of the frozen solution EPR signals are ∼1.4 times greater than their liquid solution widths. This behavior exactly parallels that observed for $[Zn_2U]^+$ indicating that the torsional constraints do not affect the physical processes which control the EPR line widths in the monocations of the bis-zinc dimeric arrays.

(3) The liquid solution EPR spectra of $[Zn_2M]^{2+}$ and $[Zn_2B]^{2+}$ are similar to those of $[Zn_2U]^{2+}$ in that their signals are narrow (∼3.5 G) and no hyperfine structure is resolved. There is no evidence for EPR signals characteristic of a triplet state[35] for either of the dications of the torsionally constrained complexes. This observation indicates that the spin−spin interactions in these biradicals are weak as is also the case for dications of the zinc−free base dimeric arrays. Despite the similarities in the liquid solution EPR spectra of the dications of the bis-zinc arrays, the temperature dependence of their signals and their frozen solution spectra are dramatically different. In the case of $[Zn_2U]^{2+}$, the width of the EPR signal observed in frozen solution (∼3.8 G) is comparable to or slightly broader than that observed in liquid solution (∼3.5 G). This behavior is similar to that observed for $[ZnFbU]^{2+}$ (∼5.9 versus ∼4.5 G). In contrast, the frozen solution EPR signals observed for both $[Zn_2M]^{2+}$ and $[Zn_2B]^{2+}$ are considerably narrower than those observed for these arrays in liquid solution. The line narrowing is particularly dramatic in the case of $[Zn_2B]^{2+}$ which exhibits a frozen solution line width of ∼1.7 G versus ∼4.1 G in liquid solution. These results indicate that the torsional constraints in the diarylethyne linker modulate the processes which govern the EPR signatures of the dications of the bis-zinc dimeric arrays and that these processes are more significantly influenced in these arrays than in the analogous zinc−free base arrays.

The EPR spectra of the oxidation products of ZnFbZn−L and ZnFbZn−R at 295 and 100 K are shown in Figure 11. The spectra of the oxidation products of Zn_3L and Zn_3R are shown in Figure 12. In the case of the latter complexes, EPR spectra were obtained for the trications in addition to the mono- and dications. The trications of ZnFbZn−L and ZnFbZn−R could not be investigated due to the limitations of the electrochemical window of the $CHCl_3$:CH_2Cl_2 solvent mixture used for these

(34) Fajer, J.; Davis, M. S. In *The Porphyrins*; Dolphin, D., Ed.; Academic Press: New York, 1979; Vol. IV, pp 197−256.

(35) (a) Wertz, J. E.; Bolton, J. R. *Electron Spin Resonance: Elementary Theory and Practical Applications*; McGraw-Hill: New York, 1972; pp 223−257. (b) Carrington, A.; McLachlan, A. D. *Introduction to Magnetic Resonance*; Harper and Row: New York, 1967; pp 115−131.

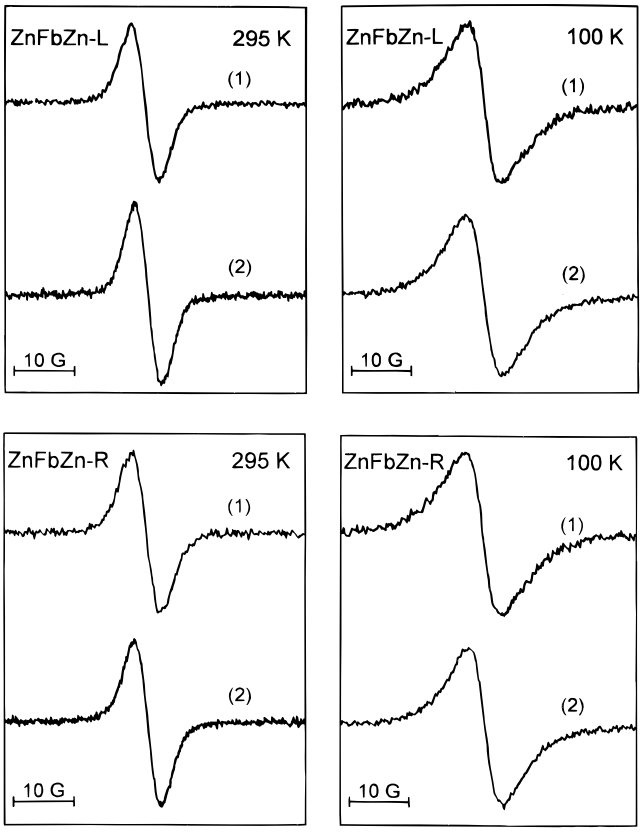

Figure 11. EPR spectra of the mono- (1) and dications (2) of ZnFbZn−L and ZnFbZn−R obtained at 295 and 100 K.

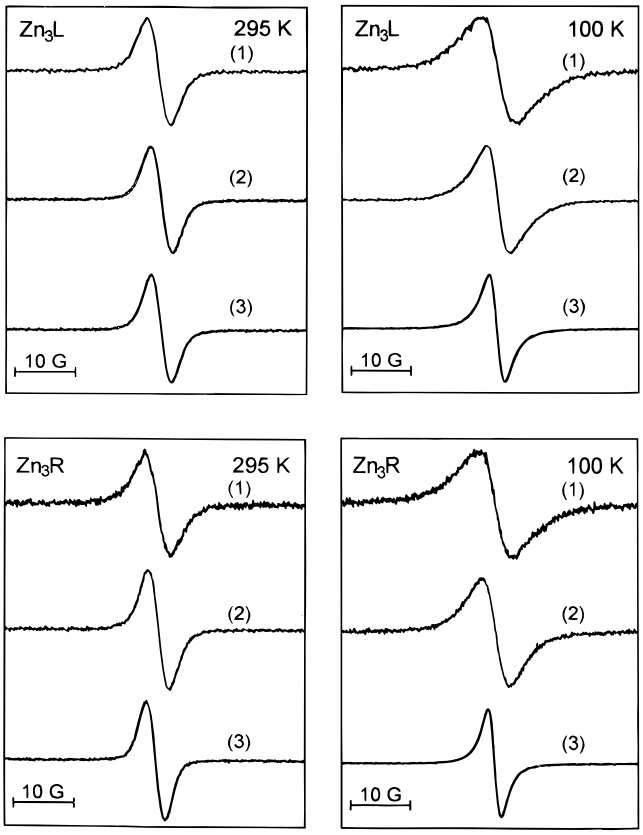

Figure 12. EPR spectra of the mono- (1), di- (2), and trications (3) of Zn_3L and Zn_3R obtained at 295 and 100 K.

complexes. The temperature dependence of the peak-to-peak line widths of the EPR signals of the various oxidation products of the trimeric arrays is listed in Table 3. The EPR spectra of the oxidized trimeric arrays were examined as a function of sample concentration and found to be independent of concentration in the range used for the experiments. Consequently, the different spectral features exhibited by the various complexes are intrinsic and cannot be ascribed to intermolecular interactions.

Examination of the EPR signatures for the cations of the various trimeric arrays reveals the following features:

(1) The spectral signatures of the analogous cations of ZnFbZn−L and ZnFbZn−R are essentially identical to one another at all temperatures. This is also the case for analogous cations of Zn_3L and Zn_3R. None of the multiply oxidized trimeric arrays exhibit evidence for triplet (or higher multiplet)[35] EPR signals in either the $g = 2$ or 4 regions. Like the RR data, these observations indicate that the linear versus right-angle arrangement of the porphyrins in the trimeric arrays has no influence on the properties which govern the EPR signatures.

(2) The temperature dependences exhibited by the EPR signals of $[ZnFbZn-L]^+$ and $[ZnFbZn-R]^+$ are very similar to those of the $[Zn_2U]^+$ (cf. Tables 2 and 3). [It should be noted that the absolute EPR line widths of the cations of the dimeric and trimeric arrays cannot be directly compared because the solvents used for the studies are different (vide infra).] In particular, the EPR signals of $[ZnFbZn-L]^+$ and $[ZnFbZn-R]^+$ broaden upon freezing the solution and exhibit line widths ∼1.4 times greater than those observed in liquid solutions (∼6.4 versus ∼4.5 G). In contrast, the temperature dependence of the EPR line widths of $[ZnFbZn-L]^{2+}$ and $[ZnFbZn-R]^{2+}$ is different from that of $[Zn_2U]^{2+}$. In liquid solution, the EPR signals of $[ZnFbZn-L]^{2+}$ and $[ZnFbZn-R]^{2+}$ are relatively narrow (∼4.0 G) but broaden considerably upon freezing the solution (∼6.4 G). In the case of $[Zn_2U]^{2+}$, the signals do not change appreciably upon solvent freezing (∼4.0 versus ∼3.8 G). These observations indicate that the processes which modulate the EPR signals in the monocations are similar in the dimeric and trimeric arrays whereas those which govern the line widths in the dications are somewhat different.

(3) The liquid solution EPR line widths of $[Zn_3L]^+$ and $[Zn_3R]^+$ (∼3.7 G) are somewhat narrower than those of $[ZnFbZn-L]^+$ and $[ZnFbZn-R]^+$ (∼4.5 G); however, the frozen solution line widths are comparable in all four trimeric monocations (∼6.4 G). Accordingly, the freezing-induced increase in the EPR line widths of $[Zn_3L]^+$ and $[Zn_3R]^+$ is a factor of ∼1.7 versus ∼1.4 for $[ZnFbZn-L]^+$ and $[ZnFbZn-R]^+$ (and $[Zn_2U]^+$). The liquid solution EPR line widths of $[Zn_3L]^{2+}$ and $[Zn_3R]^{2+}$ (∼3.5 G) are also narrower than those of $[ZnFbZn-L]^{2+}$ and $[ZnFbZn-R]^{2+}$ (∼4.0 G). The temperature dependence of the linewidths is also different in the dications of the all-zinc versus bis-zinc−free base trimers. In the case of $[Zn_3L]^{2+}$ and $[Zn_3R]^{2+}$, the EPR signals broaden only slightly upon freezing the solvent (from ∼3.5 to ∼4.5 G). This behavior can be contrasted with that observed for $[ZnFbZn-L]^{2+}$ and $[ZnFbZn-R]^{2+}$ whose signals exhibit considerable broadening upon solvent freezing (vide infra). On the other hand, the temperature dependence of the EPR signals $[Zn_3L]^{2+}$ and $[Zn_3R]^{2+}$ is similar to that observed for $[Zn_2U]^{2+}$. In the case of $[Zn_3L]^{3+}$ and $[Zn_3R]^{3+}$, the liquid solution EPR signals are narrower still (∼3.3 G) than those of the mono- (∼3.7 G) or dications (∼3.5 G). For both $[Zn_3L]^{3+}$ and $[Zn_3R]^{3+}$, the EPR signals narrow further upon freezing the solvent (∼2.1−2.6 G). This latter behavior parallels that previously observed for multiply oxidized pentameric zinc porphyrin arrays.[18] Accordingly, similar processes most likely govern the EPR line widths in all zinc trimeric and pentameric arrays.

Table 3. Temperature Dependence of the Peak-to-Peak Line Widths[a] for the 1-, 2-, and 3-Electron Oxidation Products of Trimeric Arrays

	ZnFbZn-R		ZnFbZn-L		Zn_3R		Zn_3L			
temp (K)	1	2	1	2	1	2	3	1	2	3
100	6.4	6.1	6.4	6.4	6.4	4.4	2.1	6.3	4.3	2.6
130	6.4	6.1	6.4	6.4	6.4	4.4	2.1	6.3	4.3	2.6
160	6.4	6.1	6.4	6.4	6.4	4.4	2.1	6.3	4.3	2.6
180	6.4	6.1	6.4	6.4	6.4	4.4	2.1	6.3	4.3	2.6
210	4.9	4.6	4.9	4.6	4.4	4.0	3.6	4.7	4.0	3.6
240	4.9	4.3	4.9	4.3	4.2	3.9	3.4	4.7	3.9	3.5
270	4.5	4.0	4.5	4.1	4.0	3.6	3.1	4.2	3.7	3.3
295	4.5	4.0	4.5	4.1	3.7	3.5	3.1	3.8	3.5	3.3

[a] The line widths are ±0.1 G.

IV. Discussion

A key aspect in designing efficient molecular photonic devices is to achieve electronic interactions among the pigments such that energy transfer prevails while deleterious electron-transfer quenching reactions are avoided. The diarylethyne linker appears well suited for this purpose owing to the fact that highly efficient energy transfer is observed in porphyrinic arrays containing this linkage (>90% between adjacent pigments[6a]). Concomitantly, there is no evidence for electron transfer. The transient absorption studies reported in Paper 2 of this series[19] indicate that the rates of energy transfer are much faster than those expected for a Förster process (resonance energy transfer).[36] Accordingly, the energy transfer must proceed predominantly via a Dexter-type mechanism (electron exchange)[37] and must be mediated by the diarylethyne linker. This mechanism is also probed by the hole/electron hopping rates in the cations of the arrays. As was noted, these latter rates are not expected to be equal to the rates of electron transfer in the excited states of the neutrals; however, they do provide some measure of the factors which control this type of process.

The fact that through-bond rather than through-space interactions appear to dominate electronic communication in diarylethyne-linked multiporphyrin arrays provides the synthetic chemist much greater flexibility in the design of molecular photonic devices. In particular, this feature affords the opportunity to tune the specific properties of the molecular device via manipulation of the structural and electronic characteristics of the individual or constituent components (porphyrins and/or linker) of the array. In the present work, we have investigated how two types of structural modification influence the degree of electronic communication. The first is the introduction of torsional constraints between the porphyrin ring(s) and diaryl groups in the dimeric arrays. The second is the variation in the number of bonds which mediate the electronic communication in linear versus right-angle trimers. The shortest pathway between the two terminal porphyrins in the former trimer involves 30 bonds whereas that in the latter involves 26 bonds (beginning on the *meso*-aryl bond of the linker and proceeding through the bonds involving the pyrrole nitrogens of the central porphyrin). These structural modifications could affect the communication in the ground and/or excited electronic states. The torsional constraints clearly affect the excited-state communication as is evidenced by the different energy-transfer rates measured for the dimeric arrays via transient spectroscopy.[19] These latter experiments do not, however, provide information on ground-state communication. Although ground-state communication is not directly pertinent to energy transfer, it provides another view of the electronic communication which occurs in the arrays. No additional information is currently available concerning the effects of geometrical arrangement of the porphyrin constituents on the electronic communication. [Transient absorption data are available on linear but not the right-angle trimers.[19]] In the sections that follow, we first discuss excited-state electronic communication and then proceed with a description of ground-state communication.

A. Excited-State Electronic Communication. The porphyrin−porphyrin electronic interactions in both the dimeric and trimeric arrays are weak as manifested by their slightly red-shifted and/or split B-state absorption bands. For the dimeric arrays, the variation in the degree of torsional constraint has no discernible effect on the absorption characteristics. For the trimeric arrays, subtle differences can be seen in the B-state absorption region of the linear versus right-angle complexes, but nothing which suggests significant differences in the degree of electronic interaction. These observations suggest that the structural variations do not result in large changes in the degree of electronic communication in the arrays. This is not surprising given that the electronic interactions are relatively small in all of the diarylethyne-linked arrays. Accordingly, the static optical spectra are not reliable indicators of electronic perturbations which can have a significant impact on the energy-transfer characteristics of the arrays.

Unlike the optical spectra, the RR scattering characteristics of the arrays appear to reflect changes in the degree of electronic commmunication. In particular, the RR intensities of the ν_{aryl} and $\nu_{C\equiv C}$ modes monotonically decrease as the degree of torsional constraint increases. For the arrays containing the bis-hindered linkers, the RR enhancements of the ν_{aryl} and $\nu_{C\equiv C}$ modes are comparable to those typically observed for tetraarylporphyrins which do not contain this group.[24] As was previously noted, the ν_{aryl} and $\nu_{C\equiv C}$ modes are unusually intense in arrays containing the unhindered linker. The large RR intensities observed for the ν_{aryl} vibrations of these porphyrins are attributed to the aryl ring bearing the ethyne group assuming a more coplanar excited-state conformation with the porphyrin macrocycle than is typically observed.[18] The rotation of the aryl group toward the porphyrin plane increases the conjugation between the π-electron systems of the two rings which, in turn, provides a mechanism for the RR enhancement of $\nu_{C\equiv C}$ which is conjugated with the π-system of the aryl ring. The ground-state torsional angles of all the arylethyne porphyrins are thought to be similar to one another and similar to those of other tetraarylporphyrins (in which the torsional angles are always 45° or more[38]). Accordingly, the loss of RR intensity for ν_{aryl} and $\nu_{C\equiv C}$ modes in the torsionally constrained dimers reflects the fact that the *ortho*-substituted aryl ring in these systems is comparatively restricted from assuming a more coplanar conformation in the excited state.

(36) Förster, Th. *Ann. Phys.* **1948**, *2*, 55−75.
(37) Dexter, D. L. *J. Chem. Phys.* **1953**, *21*, 836−850.
(38) (a) Scheidt, W. R. In *The Porphyrins*; Dolphin, D., Ed.; Academic Press: New York, 1978; Vol. III, pp 463−512. (b) Meyer, E. F., Jr.; Cullen, D. L. *Ibid*., pp 513−530.
(39) Gust, D.; Moore, T. A.; Makings, L. R.; Liddell, P. A.; Nemeth, G. A.; Moore, A. L. *J. Am. Chem. Soc.* **1986**, *108*, 8028−8031.

The qualitative similarity between the trends in the RR enhancement patterns of the ν_{aryl} and $\nu_{C\equiv C}$ bands and the energy-transfer rates of the various torsionally constrained dimers suggests that the degree of extended conjugation in the excited state is the key factor in mediating both of these processes. In particular, both the RR intensities of the ν_{aryl} and $\nu_{C\equiv C}$ bands and the energy-transfer rates monotonically decrease with increasing torsional constraint. [Recall that the energy-transfer times for the arrays containing the unhindered, mono-hindered (both distal and proximal), and bis-hindered linkers are $\sim(24\ ps)^{-1}$, $\sim(46\ ps)^{-1}$, and $\sim(88\ ps)^{-1}$, respectively.[19]] It should be noted that the measured energy-transfer rates involve the Q-states whereas the RR experiments reported herein involve the B-states. It is not possible to obtain Q-state RR data for the zinc-containing arrays owing to the large amount of fluorescence. However, in previous experiments on a copper substituted arylethyne porphyrin, we found that large RR enhancements are also observed for the ν_{aryl} and $\nu_{C\equiv C}$ modes with Q-state excitation.[18]

The effect of temperature on the RR intensities of the ν_{aryl} and $\nu_{C\equiv C}$ modes is particularly curious. At low temperature, these modes gain significant intensity in the dimeric arrays containing the bis-hindered linker but not in the arrays containing the unhindered or mono-hindered linkers. The origin of this effect is not certain owing to the large number of factors which could influence the RR intensities. For example, the position of the energy minimum along the torsional coordinate in either the ground or excited-electronic state could be more substantially perturbed in frozen solution for arrays containing the bis-hindered linker than for arrays containing the other linkers. Alternatively, the temperature effect may arise from changes in the shape (rather than the position of the minimum) of the potential for the bis-hindered versus the other types of arrays. In the absence of additional information, it is not possible to determine which of these (or other) factors might be important. It should also be noted that there is no obvious correlation between the effects of temperature on the RR intensities of the ν_{aryl} and $\nu_{C\equiv C}$ modes and the energy-transfer rates. If anything, there appears to be an anticorrelation. In particular, the energy-transfer rate for the array containing the unhindered linker is slowed at low temperatures whereas the rate for the array containing the bis-hindered linker is not altered.[19]

The fact that the RR intensity enhancement patterns of the ν_{aryl} and $\nu_{C\equiv C}$ modes of the linear and right-angle trimers are very similar suggests that the geometrical arrangement of the porphyrins in the array has little influence on the degree of extended excited-state conjugation. This in turn suggests that the number of bonds in the pathway has little effect on this property. This result is not particularly surprising given that the additional bonds present in the linear versus right-angle trimers are all internal to the central porphyrin ring. The highly conjugated nature of the porphyrin π-electron system results in essentially identical coupling between groups attached at any pair of *meso*-positions (5,10 or 5,15 giving right-angle or linear geometries) on the central porphyrin. In this regard, Gust et al. have prepared carotenoid−porphyrin−quinone triads in linear and right-angle geometries and have found that these exhibit identical charge-recombination rates.[39] Although the energy-transfer rates have not been measured for our linear versus right-angle trimers, the results of the RR (and other experiments (vide infra)) suggest that the geometrical arrangement of the constituent porphyrins will not significantly affect these rates. This would not be the case if through-space electronic communication were important given that the peripheral porphyrins are much closer in right-angle versus linear trimers. In this regard, however, initial transient absorption studies on linear zinc−zinc−free base trimers indicate very fast net energy transfer ($\sim$100 ps),[19] commensurate with through-bond electronic communication.

Finally, we note that although the diarylethyne linker appears particularly well suited for the mediation of efficient energy transfer, a different type of linker (phenyl−amide−phenyl) has also been shown to promote rapid ($\sim$43 ps), efficient energy transfer between zinc and free-base porphyrins.[40] This linker has the same number of bonds in the communication pathway as the diarylethyne but the amide and ethyne clearly have different electronic structures. Together these observations indicate that there is considerable versatility in the design of efficient energy transfer systems.

B. Ground-State Electronic Communication. Our approach for assessing ground-state interactions in the torsionally constrained dimers and linear versus right-angle trimers involves electrochemical formation of cation radicals and EPR studies. The rationale for these studies and the interpretation of the data parallels that described in our previous work on dimeric and pentameric arrays.[18] Together, the electrochemical and EPR data provide information concerning the energies, hole/electron hopping rates, and spin-exchange interactions in the arrays. In general, the redox properties of the torsionally constrained dimers and linear and right-angle trimers are similar to those we have previously observed for other multiporphyrin arrays. In particular, the electrochemical studies indicate that while the one-electron redox potentials for the zinc porphyrins in arrays containing multiple zinc porphyrins are similar, they are not identical. The EPR spectra of the oxidized assemblies exhibit complex temperature-dependent signatures that reflect interporphyrin interactions. All of these features can be explained by hole/electron hopping and/or spin-exchange mechanisms.[41] In the case of the zinc−free base and bis-zinc dimers, either one or the other mechanism is operative for a particular cation. This is also the case for certain cations of the trimeric arrays; however, for others, both mechanisms are simultaneously operative. The fact that the EPR spectra of all the cations are independent of concentration indicates that the hole/electron hopping and exchange is intramolecular rather than intermolecular. These processes are also necessarily mediated through the arylethyne linkers because the interporphyrin separations are extremely large. The edge-to-edge separations of nearest-neighbor porphyrins are $\sim$13 Å. In the right-angle trimeric arrays, the closest approach edge-to-edge distance between peripheral porphyrins is $\sim$20 Å. The rates of through-space hole/electron hopping or magnitude of spin exchange over such distances are expected to be at least 10^8 times less than those observed for the arrays (vide infra).[41a,42] The rate of interporphyrin hole/electron hopping is slow on the electronic and vibrational time scales (10^{-13}−10^{-15} s); consequently, the absorption and RR spectra are a superposition of the spectra of the individual components. In contrast, the processes are fast or comparable to the relatively long time scales that determine

(40) Gust, D.; Moore, T. A.; Moore, A. L.; Gao, F.; Luttrull, D.; DeGraziano, J. M.; Ma, X. C.; Makings, L. R.; Lee, S.-J.; Trier, T. T.; Bittersmann, E.; Seely, G. R.; Woodward, S.; Bensasson, R. V.; Rougée, M.; De Schryver, F. C.; Van der Auweraer, M. *J. Am. Chem. Soc.* **1991**, *113*, 3638−3649.

(41) (a) Atherton, N. M. *Principles of Electron Spin Resonance*; Ellis Horwood: New York, 1993; pp 253−263. (b) Bencini, A.; Gatteschi, D. *Electron Paramagnetic Resonance of Exchange Coupled Systems*; Springer Verlag: Berlin, 1990.

(42) (a) Moser, C. C.; Keske, J. M.; Warncke, K.; Farid, R. S.; Dutton, P. L. *Nature* **1992**, *355*, 792−796 and references therein. (b) Paddon-Row, M. N. *Acc. Chem. Res.* **1994**, *27*, 18−25 and references therein.

the EPR signatures ($10^{-6}-10^{-8}$ s); hence, the spectra deviate from simple superpositions.

Our previous studies of $[Zn_2U]^+$ revealed that, in liquid solution, the hole/electron is completely delocalized (rapid hopping) over the two zinc porphyrins on the EPR time scale.[18] This is evidenced by the fact that the ^{14}N hyperfine couplings are reduced by a factor of 2 relative to those of a monomeric porphyrin.[35] [In the case of unresolved hyperfine splittings, the peak-to-peak line width in the delocalized dimer is scaled by a factor of $2^{-1/2}$.[43]] The ^{14}N hyperfine splittings of monomeric porphyrins are on the order of 1.6 G (4.5 MHz); consequently, the hole/electron hopping rate in $[Zn_2U]^+$ is on the order of 10^7 s^{-1} or greater, but necessarily less than a typical vibrational frequency ($10^{13}-10^{14}$ s^{-1}). In frozen solution, the hole/electron hopping in $[Zn_2U]^+$ becomes slow on the EPR time scale as evidenced by the fact that the ^{14}N hyperfine couplings are comparable to those observed for a monomer. In the case of $[ZnFbU]^+$, the hole/electron is completely localized on the zinc porphyrin at all temperatures owing to the large difference in redox potentials of the zinc and free base porphyrins (Table 1). Accordingly, this dimer exhibits ^{14}N hyperfine splittings similar to those of monomeric porphyrin cations.

For the monocations of the torsionally constrained dimers, both the liquid and frozen solution EPR signatures are similar to those observed for the torsionally unconstrained analogues (Table 2). This result is anticipated for the zinc−free base dimers owing to the fact that the hole/electron is completely localized and torsional constraints should have minimal effect on the EPR signature. The fact that the EPR signatures for $[Zn_2M]^+$ and $[Zn_2B]^+$ are similar to one another and similar to those of $[Zn_2U]^+$ indicates that the rate of hole/electron hopping in both of the torsionally contrained systems is rapid in liquid solution but slow in frozen solution (on the EPR time scale). To within experimental error, the EPR data suggest that the holes/electrons in both $[Zn_2M]^+$ and $[Zn_2B]^+$ are delocalized in liquid solution. There are several possible explanations for this result: (1) The torsional constraints have no effect on the hole/electron hopping rate. (2) The torsional constraints increase the rate. (3) The torsional constraints decrease the rate but to an extent insufficient to influence the EPR signature. Of these explanations, the third would seem to be the most reasonable.

Our previous studies on $[ZnFbU]^{2+}$ and $[Zn_2U]^{2+}$ both of which contain a spin center on each porphyrin of the dimer reveal that the two spin centers interact via long-range, through-bond exchange interactions.[18] [The presence of holes on each porphyrin in the dications precludes hole/electron hopping.] The exchange interactions in $[ZnFbU]^{2+}$ and $[Zn_2U]^{2+}$ appear to be much larger than the ^{14}N hyperfine coupling (on the order of 1000 MHz) as evidenced by the degree of line narrowing observed in the EPR spectrum.[35,44,45] The exchange interactions are operative in both liquid and frozen solution and in the case of $[Zn_2U]^{2+}$ appear to be slightly larger in the latter medium.

For the dications of the torsionally constrained dimers, the liquid solution EPR signatures are similar to those observed for the torsionally unconstrained analogues (Table 2). These observations suggest that the torsional constraints do not significantly attenuate the exchange processes and that the exchange coupling remains much larger than the ^{14}N hyperfine coupling for all the dications. This also appears to be the case for the torsionally constrained zinc−free base dications in frozen solution whose EPR signatures are similar to those of the unhindered analogue. In contrast, the frozen solution EPR line widths for the torsionally constrained bis-zinc dications become progressively narrower as the degree of torsional constraint increases. This observation suggests that either the intrinsic magnitude of the exchange interaction dramatically increases in frozen solution or that dynamical processes which mitigate the exchange process in liquid solution are significantly attenuated in frozen solution. The exact origin of the increased exchange interactions in the torsionally constrained dimers is not certain. Previous EPR studies of other biradicals have shown that the exchange coupling can exhibit an extremely complex temperature (and solvent) dependence.[44] Regardless, the fact that the exchange interactions in the torsionally constrained dimers can be influenced by the medium suggests that the environmental and architectural factors can be used in concert to manipulate the electronic communication in the multiporphyrin arrays.

The features observed in the EPR spectra of all the cation radicals of trimeric arrays also can be explained by hole/electron hopping and/or spin-exchange interactions. The properties of these arrays parallel those we have previously observed for single and multiply oxidized pentameric arrays.[18] In the mono- (and more highly oxidized) cations of these latter arrays, the hole/electron hopping is rapid on the EPR time scale regardless of whether the central porphyrin is a zinc or free base porphyrin. As is the case for the dimeric arrays, the hopping process in the pentamers becomes slow on the EPR time scale upon freezing the solution. Spin-exchange processes are also operative in the multiply oxidized pentameric arrays. The exchange interactions are complicated owing to the large number of possible spin centers. However, the exchange couplings are generally larger in all-zinc pentamers than in tetra-zinc pentamers containing a central free base. The smaller exchange interactions in the latter are attributed to the fact that the hole cannot reside on the central free base porphyrin (except for the pentacation) owing to its higher oxidation potential.

For the monocations of all four trimeric arrays, a single hole/electron hops among the zinc porphyrins and hopping is the only possible line narrowing mechanism. In liquid solution, all four monocations exhibit narrow lines consistent with rapid hole/electron hopping (Table 3). In frozen solution, the EPR line widths are comparable to those of monomeric cations, indicative of a much slower hopping rate. For $[ZnFbZn-L]^+$ and $[ZnFbZn-R]^+$, the hole can only reside on the two peripheral zinc porphyrins whereas for $[Zn_3L]^+$ and $[Zn_3R]^+$ it can reside on all three zinc porphyrins. For a delocalized system, in the case of unresolved hyperfine splittings, the peak-to-peak line widths scale as $n^{-1/2}$, where n is the number of residence sites.[43] The fact that the liquid solution EPR line widths of $[Zn_3L]^+$ and $[Zn_3R]^+$ are somewhat narrower than those of $[ZnFbZn-L]^+$ and $[ZnFbZn-R]^+$ and are within experimental error of $3^{-1/2}$ and $2^{-1/2}$, respectively, is consistent with the notion of delocalization for both types of array on the EPR time scale.

For $[ZnFbZn-L]^{2+}$ and $[ZnFbZn-R]^{2+}$, only exchange processes can contribute to the EPR line shape because hole/electron hopping is precluded. The relatively narrow lines observed for these dications in liquid solution are attributed to exchange interactions. Upon freezing the solvent, the EPR line widths observed for both $[ZnFbZn-L]^{2+}$ and $[ZnFbZn-R]^{2+}$ increase considerably consistent with a decrease in the magnitude of the exchange coupling. This trend parallels that observed for $[ZnFbU]^{2+}$ (Table 2). For $[Zn_3L]^{2+}$ and $[Zn_3R]^{2+}$,

(43) Norris, J. R.; Uphaus, R. A.; Crespi, H. L.; Katz, J. J. *Proc. Natl. Acad. Sci. U.S.A.* **1971**, *68*, 625−628.

(44) Glarum, S. H.; Marshall, J. H. *J. Chem. Phys.* **1967**, *47*, 1374−1378.

(45) For a thorough discussion of exchange processes in biradicals see: Closs, G. L.; Forbes, M. D. E.; Piotrowiak, P. *J. Am. Chem. Soc.* **1992**, *114*, 3285−3294.

both hole/electron hopping and exchange processes can occur. Both processes most likely contribute to the line narrowing observed in liquid solution. In contrast the relatively narrow lines observed in frozen solution are most likely due exclusively to exchange processes. In the case of $[Zn_3L]^{3+}$ and $[Zn_3R]^{3+}$, only exchange processes are operative. These lead to narrow EPR lines in both liquid and frozen solution.

V. Summary and Conclusions

The electrochemical and spectroscopic studies reported herein indicate that the excited-state electronic communication in the diarylethyne-linked porphyrin arrays can be modulated via control of the degree of coplanarity between the aryl groups in the linker and porphyrin rings. In contrast, the excited-state communication does not appear to be at all sensitive to linear versus right-angle arrangements of the porphyrins in the array. For the ground state, the electronic communication is not strongly influenced by either the degree of aryl group−porphyrin coplanarity or the geometrical arrangement of the porphyrin pigments. The fact that the excited-state electronic communication can be tuned via manipulation of the structural and/or electronic properties of the linker opens new directions in the strategy for designing molecular photonic devices based on the diarylethyne-linker architecture. For example, our initial design for a molecular photonic wire was based on a diarylethyne linker with *ortho*-methyl groups.[6b] Although the overall energy-transfer efficiency of the wire is ∼76%, the static spectroscopic studies reported herein along with the dynamic studies reported in Paper 2 of this series[19] indicate that the *ortho*-methyl groups on the linker decrease the extent of excited-state electronic communication and thereby reduce the overall efficiency of the wire. A similar photonic wire containing unhindered linkers should be capable of efficiencies greater than 90%. Accordingly, this design modification will be implemented in next generation versions of the molecular wire.

The molecular design of the multiporphyrin arrays was built around the notion that the porphyrins must be brought close enough to permit rapid energy transfer but held sufficiently far apart to preclude competing electron-transfer quenching reactions. The center-to-center distance of ∼20 Å provided by the diarylethyne linker achieves this separation. In addition, the linker incorporates other important design and synthesis features including facial-encumbering groups in order to achieve enhanced organic solubility and the use of a building block strategy that enables precise definition of the metalation state of each porphyrin in an array. The relatively slow rates of hole/electron transfer in the diarylethyne linked multiporphyrin arrays ($\sim 10^7$ s^{-1} in the cations) compared with the much faster rates of energy transfer ($\sim 10^{10}$ s^{-1} in the neutrals)[19] suggest that the molecular designer has a window in which the rates of energy transfer can be tuned without compromising the efficiency of the system via electron-transfer quenching reactions. This property has proven critical in our initial demonstration of molecular photonic gates based on the diarylethyne-linked multiporphyrin design motif.[6c] In the future, we anticipate that this element of the molecular architecture will provide robust access to other multiporphyrin arrays that can be tailored in versatile ways in order to maximize functional characteristics.

Acknowledgment. This work was supported by the LACOR Program (D.F.B.) and Subcontract No. 346KK014−19C (J.S.L.) from Los Alamos National Laboratory and grants GM36243 (D.F.B.) and GM36238 (J.S.L.) from the National Institute of General Medical Sciences.

JA9616138